

EXTRACTING MANIFOLD INFORMATION FROM POINT CLOUDS

PATRICK GUIDOTTI

ABSTRACT. A kernel based method is proposed for the construction of signature (defining) functions of subsets of \mathbb{R}^d . The subsets can range from full dimensional manifolds (open subsets) to point clouds (a finite number of points) and include bounded (closed) smooth manifolds of any codimension. The interpolation and analysis of point clouds are the main application. Two extreme cases in terms of regularity are considered, where the data set is interpolated by an analytic surface, at the one extreme, and by a Hölder continuous surface, at the other. The signature function can be computed as a combination of translated kernels, the coefficients of which are the solution of a Fredholm integral equation (matrix equation in the finite dimensional case). Once it is obtained, it can be used to estimate the dimension as well as the normal and the curvatures of the interpolated manifold. The method is global and does not require the data set to be organized or structured in any particular way. It admits a variational formulation with a natural regularized counterpart, that proves useful in dealing with data sets corrupted by numerical error or noise. The underlying analytical structure of the approach is presented in general before it is applied to the case of point clouds.

1. INTRODUCTION

The main goal of this paper is to propose a method to compute geometric information about a manifold (a hypersurface, in many cases) that is merely given as a point cloud, i.e. a set of points that are assumed to be a sampling of the given manifold. While this may not always be the primary goal of manifold learning, the connection to it is obvious and warrants some discussion. Manifold learning is mainly motivated by the desire to find a “simpler” lower dimensional representation for data that, while embedded in a space of high dimension, are intrinsically of lower dimension. This is clearly the case when the data represent a discrete sample of a low dimensional manifold sitting in a high dimensional (Euclidean, for most purposes) space, but the ideas and techniques are used well beyond this “pure” setting in applications. The first attempts were historically in a (fundamentally) linear context and the core ideas were those of Principal Component Analysis (PCA) [23, 13] and Multidimensional Scaling (MDS) [25, 9]. The first attempts to find orthogonal axes along which most of the variance in the data is captured, whereas the second looks for a lower dimensional embedding that preserves the distances between the data points. In many applications of interest, however, data do not lie on a linear manifold (even in the absence of noise) and points that are close to each other in the ambient space may be far from each other on the manifold. This led to the development of methods capable of detecting the nonlinear nature of the (data) manifold. The idea is often to associate a (adjacency) graph to the data exploiting the neighborhood structure of each datum, given either by the data points found in small ball centered at the datum itself or by its k nearest neighbors (k NN). An important such method is called isomaps [24]. It approximates geodesic distance by minimum path distance on the graph before using MDS. In this way the global structure is preserved. Others are Laplacian Eigenmaps [2] and Diffusion maps [7], where eigenfunctions (vectors) of the graph Laplacian provide an embedding of the data given simply by their evaluation at the given data point for the first, or weighted evaluation (where the weights are given by “time” and the exponential decay of the modes for the corresponding heat semigroup) for the second. Diffusion maps have the advantage of uncovering any multiscale structure present, see [8, 6, 17] and of providing robustness against noisy data and/or outliers. Methods based on the graph Laplacian also admit a solid theoretical foundation

Key words and phrases. Kernel based interpolation of generalized functions, geometric properties of point clouds.

as it is known that the graph Laplacian (sometimes) converges to the Laplace-Beltrami operator of the manifold that is being sampled [3, 12] and that (carefully selected) eigenfunctions can indeed (rigorously) provide local coordinates, see [14] for the theoretical result and [15] for an implementation. Interestingly Laplacian Eigenmaps ideas and techniques have recently been exploited for the estimation of the tangent space to a manifold as an alternative to a more direct method based on (local) PCA in a way that is more robust to noise [16]. Here we take a different approach and use an optimization procedure to obtain a continuous (as opposed to discrete) defining function from which geometric quantities can be evaluated. The main advantage of the proposed approach is that it is global in nature, does not require any structure or organization of the point cloud, and can be deployed even in the presence of noise. It is often of interest to be able to deal with new points that were not part of the original data set [4]. For the proposed method, this is immediate since it produces a (approximate) defining function for the underlying manifold that can be evaluated anywhere. The presented approach borrows ideas from interpolation theory [28] and statistical regression [26]. The connection between these two points of view is discussed in more detail in [11], where the ideas are further developed and lead to (high order) discretizations of geometric operators on point clouds.

2. CONSTRUCTING (APPROXIMATE) DEFINING FUNCTIONS

2.1. Minimal Regularity. Let $\mathcal{M} \subset \mathbb{R}^d$ be a closed bounded smooth oriented manifold, which will often be taken to be a (hyper)surface, and denote by $\delta_{\mathcal{M}} \in \mathcal{E}' \subset \mathcal{S}'$ the compactly supported generalized function (tempered distribution, in fact) defined by

$$\langle \delta_{\mathcal{M}}, \varphi \rangle = \int_{\mathcal{M}} \varphi(x) d\sigma_{\mathcal{M}}(x), \quad \varphi \in C^{\infty}(\mathbb{R}^n),$$

where $d\sigma_{\mathcal{M}}$ is the volume form on \mathcal{M} . Here we use the classical notation \mathcal{E} and \mathcal{S} for the space of smooth (C^{∞}) functions and the space of rapidly decreasing smooth functions, respectively. The latter consists of functions $u \in \mathcal{E}$ for which

$$q_{k,m}(u) = \sup_{|\alpha| \leq k} \sup_{x \in \mathbb{R}^d} (1 + |x|^2)^{m/2} |\partial^{\alpha} u(x)| < \infty$$

for every $m, k \in \mathbb{N}$. Then \mathcal{E}' and \mathcal{S}' are their topological duals as locally convex spaces with seminorms given by $p_{k,m} = \sup_{|\alpha| \leq k} \sup_{x \in \bar{\mathbb{B}}(0,m)} |\partial^{\alpha} \cdot|$ and $q_{k,m}$, $k, m \in \mathbb{N}$. We are interested in finding a smooth function $u_{\mathcal{M}} : \mathbb{R}^d \rightarrow \mathbb{R}$ which has the property that

$$[u_{\mathcal{M}} = 1] \cap \mathcal{M}_{\delta} = \mathcal{M} \text{ for some } \delta > 0,$$

where \mathcal{M}_{δ} is a neighborhood (δ -fattening) of \mathcal{M} given by

$$\mathcal{M}_{\delta} = [d(\cdot, \mathcal{M}) < \delta].$$

We take two approaches to generating functions $u_{\mathcal{M}}$ with the above property characterized by two extremal choices for their global regularity. For $s \in \mathbb{R}$, let

$$H^s(\mathbb{R}^d) = \{u \in \mathcal{S}' \mid (1 + |\xi|^2)^{s/2} \hat{u} \in L^2(\mathbb{R}^d)\}$$

be the usual Bessel potential space, where \hat{u} denotes the Fourier transform of u . First we describe the “minimal regularity” case and consider the (“Laplacian Regularized”) optimization Problems

$$\operatorname{argmin}_{u \in H^{\frac{d+1}{2}}(\mathbb{R}^d), u|_{\mathcal{M}} \equiv 1} \underbrace{\frac{1}{2c_d} \|(1 - 4\pi^2 \Delta)^{\frac{d+1}{4}} u\|_2^2}_{E_0(u)} \quad (\text{LRP}_0)$$

and, for $\alpha > 0$,

$$\operatorname{argmin}_{u \in H^{\frac{d+1}{2}}(\mathbb{R}^d)} \underbrace{\left(E_0(u) + \frac{1}{2\alpha} \int_{\mathcal{M}} (u - 1)^2 d\sigma_{\mathcal{M}} \right)}_{E_{\alpha}(u)}, \quad (\text{LRP}_{\alpha})$$

where $c_d = \Gamma(d+1)/\pi^{\frac{d+1}{2}}$ and $f_{\mathcal{M}}(\cdot) d\sigma_{\mathcal{M}} = \frac{1}{|\mathcal{M}|} \int_{\mathcal{M}}(\cdot) d\sigma_{\mathcal{M}}$ for $|\mathcal{M}| = \int_{\mathcal{M}} d\sigma_{\mathcal{M}}$. The objective functionals above are denoted by E_0 and by E_{α} for $\alpha > 0$, respectively.

Lemma 2.1. *The optimization problems (LRP_{α}) , $\alpha \geq 0$, possess a unique minimizer $u_{\mathcal{M}}^{\alpha} \in H^{\frac{d+1}{2}}(\mathbb{R}^d)$. For $\alpha > 0$, the minimizer is a weak solution of the equation*

$$Au := \frac{1}{c_d} (1 - 4\pi^2 \Delta)^{\frac{d+1}{2}} u = \frac{1}{\alpha |\mathcal{M}|} (1 - u) \delta_{\mathcal{M}}, \quad (2.1)$$

i.e. a solution of the equation in \mathcal{E}' (in fact, in $H^{-\frac{d+1}{2}}(\mathbb{R}^d)$), or, explicitly it satisfies

$$\alpha \langle Au, v \rangle = \frac{\alpha}{c_d} \int_{\mathbb{R}^d} [(1 - 4\pi^2 \Delta)^{\frac{d+1}{4}} u](x) \cdot [(1 - 4\pi^2 \Delta)^{\frac{d+1}{4}} v](x) dx = \int_{\mathcal{M}} (1 - u)(x) v(x) d\sigma_{\mathcal{M}}(x),$$

for all $v \in H^{\frac{d+1}{2}}(\mathbb{R}^d)$. If $\alpha = 0$, then it holds that $Au_{\mathcal{M}}^0$ is a distribution of order 0 with $\text{supp}(Au_{\mathcal{M}}) \subset \mathcal{M}$, that is,

$$Au_{\mathcal{M}}^0 = \psi^0 \frac{1}{|\mathcal{M}|} \delta_{\mathcal{M}}, \quad (2.2)$$

for some $\psi^0 \in L^1(\mathcal{M})$, where

$$\langle \psi^0 \delta_{\mathcal{M}}, \varphi \rangle := \int_{\mathcal{M}} \psi^0(x) \gamma_{\mathcal{M}} \varphi(x) d\sigma_{\mathcal{M}}(x), \quad \varphi \in H^{\frac{d+1}{2}}(\mathbb{R}^d),$$

and $\gamma_{\mathcal{M}} \varphi$ is the trace of φ on \mathcal{M} .

Proof. It is a standard result, [1], that $H^{\frac{d+1}{2}}(\mathbb{R}^d) \hookrightarrow \text{BUC}^{1/2}(\mathbb{R}^d)$, where the latter space consists of all bounded and uniformly Hölder continuous functions on \mathbb{R}^d of order 1/2 endowed with the norm $\|\cdot\|_{\infty} + [\cdot]_{1/2}$, where

$$[u]_{1/2} = \sup_{\tilde{x} \neq x} \frac{|u(x) - u(\tilde{x})|}{|x - \tilde{x}|^{1/2}}, \quad u \in \text{BUC}^{1/2}(\mathbb{R}^d).$$

The evaluation of functions in the Bessel space at points in \mathbb{R}^d is therefore well-defined. Consequently, the constraint $u|_{\mathcal{M}} \equiv 1$ is meaningful. The energy functional E_{α} , $\alpha \geq 0$ appearing in (LRP_{α}) is convex and lower semi-continuous regardless of $\alpha \geq 0$. Convex, lower semi-continuous functionals on a Hilbert space are weakly lower semi-continuous. Coercivity is also given since bounded subsets of $H^{\frac{d+1}{2}}(\mathbb{R}^d)$ are relatively weakly compact by the Banach-Alaoglu Theorem. These properties ensure existence, which is unique since the functionals are strictly convex. For the case $\alpha = 0$ it has to be observed that minimization occurs over the closed convex (and hence weakly closed) set consisting of functions u for which $u(\mathcal{M}) = \{1\}$. Taking variations in direction of test functions $\varphi \in \mathcal{D}(\mathbb{R}^d)$ at the minimizer and using the fact that the operator $(1 - 4\pi^2 \Delta)^{\frac{d+1}{4}}$ is self-adjoint, it is seen that

$$\begin{aligned} 0 &= \frac{d}{dr} \Big|_{r=0} E_{\alpha}(u_{\mathcal{M}}^{\alpha} + r\varphi) = \frac{1}{c_d} \int (1 - 4\pi^2 \Delta)^{\frac{d+1}{4}} u_{\mathcal{M}}^{\alpha} (1 - 4\pi^2 \Delta)^{\frac{d+1}{4}} \varphi dx + \frac{1}{\alpha} \int_{\mathcal{M}} (u_{\mathcal{M}}^{\alpha} - 1) \varphi d\sigma_{\mathcal{M}} \\ &= \frac{1}{c_d} \langle (1 - 4\pi^2 \Delta)^{\frac{d+1}{4}} u_{\mathcal{M}}^{\alpha}, (1 - 4\pi^2 \Delta)^{\frac{d+1}{4}} \varphi \rangle_{L^2(\mathbb{R}^d)} + \frac{1}{\alpha} \langle u_{\mathcal{M}}^{\alpha} - 1, \varphi \rangle_{L^2(\mathcal{M})} \\ &= \langle \frac{1}{c_d} (1 - 4\pi^2 \Delta)^{\frac{d+1}{2}} u_{\mathcal{M}}^{\alpha}, \varphi \rangle_{H^{-\frac{d+1}{2}}, H^{\frac{d+1}{2}}} + \frac{1}{\alpha} \langle u_{\mathcal{M}}^{\alpha} - 1, \varphi \rangle_{L^2(\mathcal{M})}, \end{aligned}$$

which is valid for all $\alpha \geq 0$ with the understanding that the manifold term is absent when $\alpha = 0$. Taking special test functions $\varphi \in \mathcal{D}(\mathbb{R}^d \setminus \mathcal{M})$, i.e. supported away from \mathcal{M} , the second term vanishes for all $\alpha \geq 0$. This shows that

$$\text{supp}(Au_{\mathcal{M}}^{\alpha}) \subset \mathcal{M}.$$

Compactly supported distributions are known to be of finite order. Using that

$$\text{BUC}^1(\mathbb{R}^d) \not\subseteq H^{\frac{d+1}{2}}(\mathbb{R}^d) \hookrightarrow \text{BUC}(\mathbb{R}^d),$$

it is concluded that the order of the distribution $Au_{\mathcal{M}}^{\alpha}$ indeed vanishes (the space on the left consists of functions that are bounded and uniformly continuous, BUC, with all first partial derivatives enjoying the same property). When $\alpha > 0$, the energy functional contains the manifold term, so that the above gives

$$\frac{1}{c_d} \langle (1 - 4\pi^2 \Delta)^{\frac{d+1}{4}} u_{\mathcal{M}}^{\alpha}, (1 - 4\pi^2 \Delta)^{\frac{d+1}{4}} \varphi \rangle_{L^2(\mathbb{R}^d)} + \frac{1}{\alpha |\mathcal{M}|} \langle (u_{\mathcal{M}}^{\alpha} - 1) \delta_{\mathcal{M}}, \varphi \rangle_{L^2(\mathcal{M})} = 0$$

for all $\varphi \in \mathcal{D}(\mathbb{R}^d)$ and hence for all $\varphi \in H^{\frac{d+1}{2}}(\mathbb{R}^d)$, which amounts to the claimed equation in weak form. \square

Next we exploit the fact that a fundamental solution for the operator A is known. It is indeed the so-called Laplace kernel L given by $L(x) = e^{-|x|}$, $x \in \mathbb{R}^d$. This allows us to invert the operator A by convolution with L . In particular, when $\alpha > 0$, this leads to the formulation

$$\alpha u(x) = \int_{\mathcal{M}} e^{-|x-y|} (1-u)(y) d\sigma_{\mathcal{M}}(y), \quad x \in \mathbb{R}^d, \quad (2.3)$$

equivalent to (2.1)*, from which we infer that the solution $u_{\mathcal{M}}$ is known if its values on \mathcal{M} are known. This makes for a dimensional reduction akin to that obtained in interpolation via reproducing kernels where an infinite dimensional problem reduces to a finite dimensional one (see later discussion of the discrete counterpart of the current situation). Indeed, evaluating (2.3) at $x \in \mathcal{M}$, yields the integral equation of the second kind

$$\alpha \gamma_{\mathcal{M}} u + \int_{\mathcal{M}} L(\cdot - y) \gamma_{\mathcal{M}} u(y) d\sigma_{\mathcal{M}}(y) = \int_{\mathcal{M}} L(\cdot - y) d\sigma_{\mathcal{M}}(y), \quad (2.4)$$

for $\gamma_{\mathcal{M}} u$ on \mathcal{M} . When $\alpha = 0$, the identity corresponding to (2.2) yields the Ansatz

$$u_{\mathcal{M}}^0 = L * (\psi^0 \frac{1}{|\mathcal{M}|} \delta_{\mathcal{M}}). \quad (2.5)$$

Lemma 2.2. *If the density function $\psi^0 \in L^1(\mathcal{M})$ in (2.5) is known, then it holds that*

$$u_{\mathcal{M}}^0(x) = \int_{\mathcal{M}} \psi^0(y) e^{-|x-y|} d\sigma_{\mathcal{M}}(y), \quad x \in \mathbb{R}^n. \quad (2.6)$$

Proof. As observed above, the Laplace kernel $L = e^{-|\cdot|}$ is a fundamental solution of the (pseudo)differential operator $\frac{1}{c_d} (1 - 4\pi^2 \Delta)^{\frac{d+1}{2}}$ and thus it holds that

$$(L * (\psi^0 \delta_{\mathcal{M}}))(x) = \langle \tau_x(\psi^0 \delta_{\mathcal{M}}), L \rangle = \langle \psi^0 \delta_{\mathcal{M}}, \tau_x L \rangle.$$

The convolution is to be understood in the sense of distributions where τ_x is translation by x , i.e. $\tau_x f = f(\cdot - x)$ for functions and τ_x is defined by duality for distributions. \square

This lemma yields an equation for the density ψ^0 in the form

$$\int_{\mathcal{M}} \psi^0(y) e^{-|x-y|} d\sigma_{\mathcal{M}}(y) = 1, \quad x \in \mathcal{M}. \quad (2.7)$$

Remark 2.3. *We would like to point an interesting connection out with research on metric space geometry, where a quantity known as magnitude (an invariant, when available) plays an important role. For its computation, one needs a so-called weighting that parallels the density function ψ_0 in (2.7) or the coefficient vector Λ^0 in (3.2) below. While in our context, the appearance of the Laplace kernel is natural in the sense that it is determined by the choice of regularizer in the optimization problem, its use in the computation of magnitude is somewhat more mysterious. It is, however, remarkable that the very same kernel can encode some geometric information about the underlying metric space. While it would be of interest to uncover any deeper connections, these do not appear obvious and we refer*

*See the proof of (2.6) for a more detailed explanation of this.

the interested reader to the seminal papers [18, 19, 20] for the case of finite metric spaces as well as to [29, 21, 30] for the case of infinite spaces (as the limit of finite spaces or with the weight defined as a Borel measure). For so-called positive definite spaces, [22] showed that the limiting finite space approach is compatible with the infinite space one. Notice that subsets of Euclidean space are positive definite in this sense.

Equation (2.7) is a Fredholm integral equation of the first kind. Introducing a Lagrange multiplier $\Lambda : \mathcal{M} \rightarrow \mathbb{R}$ for the constraint $u|_{\mathcal{M}} \equiv 1$ in (LRP_0) yields the functional

$$E_0(u, \Lambda) = E_0(u) + \frac{1}{|\mathcal{M}|} \langle \Lambda, 1 - \gamma_{\mathcal{M}} u \rangle_{\mathcal{M}}$$

which entails that $u_{\mathcal{M}}^0$ weakly solves the equation

$$Au = \frac{1}{|\mathcal{M}|} \Lambda^0 \delta_{\mathcal{M}}$$

once the Lagrange multiplier Λ^0 is known. This provides another justification for the Ansatz and for Equation (2.7). Any solution yields a critical point of E_0 , which is necessarily a minimizer. The equation has a solution since a minimizer $u_{\mathcal{M}}^0$ of E_0 is a weak solution and it is known to exist. The density (or Lagrange multiplier) can be recovered from $Au_{\mathcal{M}}^0$ by means of Riesz representation theorem. As an equation of the first kind, (2.7) is ill-posed, while (2.4) is not, as an equation of the second kind. In fact the latter can be viewed and thought of as a regularization of the former.

Proposition 2.4. *Denoting by $u_{\mathcal{M}}^{\alpha}$ the minimizer of E_{α} for $\alpha \geq 0$, it holds that*

$$u_{\mathcal{M}}^{\alpha} \rightarrow u_{\mathcal{M}}^0 \text{ as } \alpha \rightarrow 0 \text{ in } H^{\frac{d+1}{2}}(\mathbb{R}^d).$$

Proof. Denote the infimum of E_{α} by $e_{\alpha} \geq 0$ and notice that $e_{\alpha} \leq e_0$ for $\alpha > 0$ since $u_{\mathcal{M}}^0 \in H^{\frac{d+1}{2}}(\mathbb{R}^d)$ and $E_{\alpha}(u_{\mathcal{M}}^0) = e_0$. This entails that $\|u_{\mathcal{M}}^{\alpha}\|_{H^{\frac{d+1}{2}}(\mathbb{R}^d)} \leq C < \infty$ independently of $\alpha > 0$. Weak compactness

yields a weakly convergent subsequence with limit $w \in H^{\frac{d+1}{2}}(\mathbb{R}^d)$, which, by weak lower semicontinuity of the norm, must satisfy $\frac{1}{2c_d} \|w\|_{H^{\frac{d+1}{2}}(\mathbb{R}^d)}^2 \leq e_0^{\dagger}$ and is therefore the unique minimizer $u_{\mathcal{M}}^0$. Take now $0 < \alpha_0 < \alpha_1$ and observe that

$$\begin{aligned} e_{\alpha_0} = E_{\alpha_0}(u_{\mathcal{M}}^{\alpha_0}) &\leq [\frac{1}{2\alpha_0} - \frac{1}{2\alpha_1}] \int_{\mathcal{M}} (u_{\mathcal{M}}^{\alpha_1} - 1)^2 d\sigma_{\mathcal{M}} + E_{\alpha_1}(u_{\mathcal{M}}^{\alpha_1}) \\ &\leq [\frac{1}{2\alpha_0} - \frac{1}{2\alpha_1}] \int_{\mathcal{M}} (u_{\mathcal{M}}^{\alpha_1} - 1)^2 d\sigma_{\mathcal{M}} + E_{\alpha_1}(u_{\mathcal{M}}^{\alpha_0}) \end{aligned}$$

implies that $\int_{\mathcal{M}} (u_{\mathcal{M}}^{\alpha_0} - 1)^2 d\sigma_{\mathcal{M}} \leq \int_{\mathcal{M}} (u_{\mathcal{M}}^{\alpha_1} - 1)^2 d\sigma_{\mathcal{M}}$. It follows that

$$\begin{aligned} \|u_{\mathcal{M}}^{\alpha_1}\|_{H^{\frac{d+1}{2}}(\mathbb{R}^d)} &\leq \|u_{\mathcal{M}}^{\alpha_0}\|_{H^{\frac{d+1}{2}}(\mathbb{R}^d)} - \frac{1}{2\alpha_1} [\int_{\mathcal{M}} (u_{\mathcal{M}}^{\alpha_1} - 1)^2 d\sigma_{\mathcal{M}} - \int_{\mathcal{M}} (u_{\mathcal{M}}^{\alpha_0} - 1)^2 d\sigma_{\mathcal{M}}] \\ &\leq \|u_{\mathcal{M}}^{\alpha_0}\|_{H^{\frac{d+1}{2}}(\mathbb{R}^d)}. \end{aligned}$$

Finally take any null sequence $(\alpha_n)_{n \in \mathbb{N}}$. By the above weak compactness and lower semicontinuity argument, it will have a subsequence that converges to $u_{\mathcal{M}}^0$. Since, additionally, the norm converges thanks to

$$\|u_{\mathcal{M}}^0\|_{H^{\frac{d+1}{2}}(\mathbb{R}^d)} \leq \liminf_{k \rightarrow \infty} \|u_{\mathcal{M}}^{\alpha_k}\|_{H^{\frac{d+1}{2}}(\mathbb{R}^d)} \leq \limsup_{k \rightarrow \infty} \|u_{\mathcal{M}}^{\alpha_k}\|_{H^{\frac{d+1}{2}}(\mathbb{R}^d)} \leq \|u_{\mathcal{M}}^0\|_{H^{\frac{d+1}{2}}(\mathbb{R}^d)},$$

the subsequence actually converges in norm. Since this is true for any null sequence $(\alpha_n)_{n \in \mathbb{N}}$ (with the same limit $u_{\mathcal{M}}^0$), the whole family converges in norm as claimed. \square

[†]We can work with the norm given by $\|u\|_{H^{\frac{d+1}{2}}(\mathbb{R}^d)} = \|(1 + 4\pi^2|\xi|^2)^{\frac{d+1}{4}} \hat{u}\|_{L^2(\mathbb{R}^d)}$

This natural regularization will prove very useful in numerical applications.

Proposition 2.5. *Using the same Ansatz*

$$u_{\mathcal{M}}^{\alpha} = \int_{\mathcal{M}} \Lambda^{\alpha}(y) e^{-|\cdot-y|} d\sigma_{\mathcal{M}}(y) \quad (2.8)$$

when $\alpha > 0$, it holds that

$$u_{\mathcal{M}}^{\alpha}|_{\mathcal{M}} = \int_{\mathcal{M}} \Lambda^{\alpha}(y) e^{-|\cdot-y|} d\sigma_{\mathcal{M}}(y) = 1 - \alpha \Lambda^{\alpha},$$

i.e. the validity of an equation for the density Λ^{α} given by

$$(\alpha + \mathcal{L})\Lambda = 1, \text{ where } \mathcal{L}\Lambda := \int_{\mathcal{M}} e^{-|\cdot-y|} \Lambda(y) d\sigma_{\mathcal{M}}(y) \quad (2.9)$$

Proof. It follows from the Ansatz and from (2.1) that

$$\frac{1}{|\mathcal{M}|} \alpha \Lambda \delta_{\mathcal{M}} = \frac{1}{|\mathcal{M}|} (1 - u_{\mathcal{M}}^{\alpha}|_{\mathcal{M}}) \delta_{\mathcal{M}},$$

which yields an equation for the densities amounting to (2.9). \square

Remark 2.6. *Representation (2.8) and equation (2.9) are the most convenient for use in numerical calculations (and will be used in the numerical experiments presented later).*

Remark 2.7. *The representations (2.3) and (2.6) show that*

$$u_{\mathcal{M}}^{\alpha} \in C^{\infty}(\mathbb{R}^d \setminus \mathcal{M}) \cap H^{\frac{d+1}{2}}(\mathbb{R}^d),$$

and therefore has generically smooth level sets away from \mathcal{M} . While \mathcal{M} is itself a level set, its regularity is clearly what it is. Notice that, while $u_{\mathcal{M}}^{\alpha}$ is smooth away from \mathcal{M} , its low global regularity allows for a sharp transition in values moving away from \mathcal{M} .

2.2. High Regularity. Inspired by the variational problems (LRP₀) we try to find a high regularity $u_{\mathcal{M}}^0 \in C^{\infty}(\mathbb{R}^d)$ by considering the problem

$$\begin{cases} u_t - \Delta u = 0, & \text{in } (0, \infty) \times \mathbb{R}^d, \\ u(0, \cdot) = \frac{\pi^{\frac{d}{2}}}{|\mathcal{M}|} \psi^0 \delta_{\mathcal{M}}, & \text{in } \mathbb{R}^d. \end{cases} \quad (2.10)$$

Its solution $u \in C^{\infty}((0, \infty) \times \mathbb{R}^d)$ is analytic and given by

$$u(t, x) = \frac{1}{(4t)^{\frac{d}{2}}} \int_{\mathcal{M}} e^{-|x-y|^2/4t} \psi^0(y) d\sigma_{\mathcal{M}}(y), \quad (t, x) \in (0, \infty) \times \mathbb{R}^d.$$

as follows from knowledge of the heat kernel. We obtain a defining function in the form $u_{\mathcal{M}}^0 = u(\frac{1}{4}, \cdot)$ for \mathcal{M} by imposing the condition

$$u\left(\frac{1}{4}, x\right) = 1, \quad x \in \mathcal{M},$$

which, again, amounts to an integral equation of the first kind and reads

$$\int_{\mathcal{M}} e^{-|x-y|^2} \psi^0(y) d\sigma_{\mathcal{M}}(y) = 1, \quad x \in \mathcal{M}. \quad (2.11)$$

Changing the initial datum to $\frac{\pi^{\frac{d}{2}}}{\alpha|\mathcal{M}|} [1 - u(\frac{1}{4}, \cdot)] \delta_{\mathcal{M}}$ for $\alpha > 0$, which “penalizes” deviation from the value 1, leads the corresponding regularized problem

$$\alpha u_{\mathcal{M}}^{\alpha}(x) + \int_{\mathcal{M}} e^{-|x-y|^2} u_{\mathcal{M}}^{\alpha}(y) d\sigma_{\mathcal{M}}(y) = \int_{\mathcal{M}} e^{-|x-y|^2} d\sigma_{\mathcal{M}}(y), \quad x \in \mathcal{M}. \quad (2.12)$$

Similar to the case of the Laplace kernel, for the Gauss kernel, we can make the Ansatz

$$u_{\mathcal{M}}^{\alpha}(x) = \int_{\mathcal{M}} \Lambda^{\alpha}(y) e^{-|x-y|^2} d\sigma_{\mathcal{M}}(y), \quad x \in \mathbb{R}^d,$$

derive the regularized equation

$$(\alpha + \mathcal{G})\Lambda^{\alpha} = 1, \text{ where } \mathcal{G}\Lambda^{\alpha} = \int_{\mathcal{M}} e^{-|\cdot-y|^2} \Lambda^{\alpha}(y) dy, \quad (2.13)$$

and observe that $u_{\mathcal{M}}^{\alpha} = 1 - \alpha\Lambda^{\alpha}$ on \mathcal{M} . In both frameworks, the minimal regularity and the smooth ones, one obtains a defining function when $\alpha = 0$ and an approximate defining function when $\alpha > 0$. As we shall demonstrate later, even an approximate defining function can play an important role in search of geometric information from data sets.

Remark 2.8. *A formal but maybe more transparent way to interpret the smooth approach just described is to introduce the energy functional*

$$G_{\alpha}(u) = \frac{1}{2} \|e^{-\frac{1}{8}\Delta} u\|_{L^2(\mathbb{R}^d)}^2 + \frac{\pi^{d/2}}{2\alpha} \int_{\mathcal{M}} (u - 1)^2 d\sigma_{\mathcal{M}},$$

where the manifold term is replaced by the constraint $u|_{\mathcal{M}} \equiv 1$ when $\alpha = 0$. Formally its Euler equation is

$$e^{-\frac{1}{4}\Delta} u = \frac{\pi^{d/2}}{\alpha|\mathcal{M}|} (1 - u) \delta_{\mathcal{M}}$$

Remark 2.9. *While the approach described so far is easier to understand mathematically for closed compact orientable hypersurfaces \mathcal{M} , it only requires the set \mathcal{M} to admit integration over it. Numerical experiments will be shown later.*

2.3. The Kernels and the Equations. An important property of the Laplace and the Gauss kernels is their positive definiteness in the sense that the matrix

$$[K(x^i - x^j)]_{1 \leq i, j \leq m}, \quad K = L, G,$$

is positive definite for any choice of m distinct points x^1, \dots, x^m in \mathbb{R}^d and any choice of $m \in \mathbb{N}$. This follows from Bochner's Theorem as the Fourier transforms \hat{L} and \hat{G} of these kernels are positive and integrable functions. At the continuous level, given a compact orientable smooth manifold $\mathcal{M} \subset \mathbb{R}^d$, the right-hand sides of (2.7) and of (2.11) define an integral operator \mathcal{K} with kernel $K = L, G$

$$\mathcal{K}\psi = \int_{\mathcal{M}} K(\cdot - y) \psi(y) d\sigma_{\mathcal{M}}(y), \quad \psi \in C(\mathbb{R}^d) \subset L^2(\mathcal{M}).$$

Noticing that

$$\langle \psi, \mathcal{K}\psi \rangle_{L^2(\mathcal{M})} = \langle \psi \delta_{\mathcal{M}}, K * (\psi \delta_{\mathcal{M}}) \rangle_{\mathcal{E}'_0, \mathcal{E}_0},$$

where the duality pairing on the right-hand side is that between compactly supported measures (zero order distributions) and continuous functions. Using (a generalization of) Plancherel's Theorem in inner product form, we see that

$$\langle \psi, \mathcal{K}\psi \rangle_{L^2(\mathcal{M})} = \langle \widehat{\psi \delta_{\mathcal{M}}}, \widehat{K} \widehat{\psi \delta_{\mathcal{M}}} \rangle_{L^2(\mathbb{R}^d)} > 0,$$

by the Paley-Wiener Theorem for compactly supported distributions and by the positivity and integrability (decay properties) of the Fourier transform of the kernel K . Thus there cannot exist a nontrivial function ψ in the nullspace of \mathcal{K} and equations (2.7) and (2.11) are uniquely solvable. As \mathcal{K} is a compact operator, the inverse is clearly unbounded and the problems ill-posed. In this sense (2.4) and (2.12) can be thought of as regularizations of (2.7) and (2.11), respectively.

3. THE DISCRETE COUNTERPART: POINT CLOUDS

We now turn our attention to sets of points (point clouds) that are assumed to be an exact or corrupted sample of the points of a manifold $\mathcal{M} \subset \mathbb{R}^d$, where, in the later experiments, $d = 2, 3$. Let $\mathbb{X} \subset \mathbb{R}^d$ denote a finite subset of distinct points (possibly sampled from an underlying manifold \mathcal{M}) which we think as listed, i.e. $\mathbb{X} = \{x^i \mid i = 1, \dots, m\}$, but where the order has no particular meaning. If this is all the information we are given about the manifold \mathcal{M} , it is natural to use these points as collocation points to approximate the various continuous quantities and equations of the previous section. In particular, it is natural to approximate the normalized measure

$$\frac{1}{|\mathcal{M}|} \delta_{\mathcal{M}} \simeq \frac{1}{m} \sum_{i=1}^m \delta_{x^i}, \quad (3.1)$$

by the empirical measure obtained from \mathbb{X} . Then equations (2.7) and (2.11) can be approximated by

$$\frac{1}{m} \sum_{k=1}^m K(x^i - x^k) \Lambda^0(x^k) = 1, \quad i = 1, \dots, m. \quad (3.2)$$

and equations (2.9) and (2.13) by

$$\alpha \Lambda_m^\alpha(x^i) + \frac{1}{m} \sum_{k=1}^m K(x^i - x^k) \Lambda^\alpha(x^k) = 1, \quad i = 1, \dots, m, \quad (3.3)$$

where K is the Laplace kernel L and Gauss kernel G , respectively. Both these kernels are positive definite and thus the matrix

$$\mathbb{R}^{m \times m} \ni M = [K(x^i - x^k)]_{1 \leq i, k \leq m} \quad (3.4)$$

is positive definite and hence invertible. Denoting the discrete density by $\Lambda_m^\alpha \in \mathbb{R}^m$ (which can be thought of as an approximation for $\Lambda^\alpha(x^k)$, $k = 1, \dots, m$) we obtain the (approximate when $\alpha > 0$) signature (defining) function of the point cloud \mathbb{X} by

$$u_{\mathbb{X}}(x) = \frac{1}{m} \sum_{k=1}^m \Lambda_m^{\alpha, k} K(x - x^k), \quad x \in \mathbb{R}^d, \quad (3.5)$$

which has the important advantage of being defined and numerically computable everywhere.

Proposition 3.1. *The signature function $u_{\mathbb{X}}$ depends continuously on the data set \mathbb{X} with respect to the $H^r(\mathbb{R}^d)$ norm for $r = \frac{d+1}{2}$, when using the Laplace kernel and any $r \in \mathbb{N}$, when using the Gauss kernel. More precisely, the map*

$$(x^1, \dots, x^m) \mapsto u_{\mathbb{X}}, \quad \mathbb{R}^m \rightarrow H^r(\mathbb{R}^d),$$

where $\mathbb{X} = \{x^1, \dots, x^m\}$, is continuous.

Proof. We consider the case of the Laplace kernel first. The claim follows from the fact that, once the values of $u_{\mathbb{X}}$ on \mathbb{X} are established, equations (2.1)-(2.2) can be used together with the continuous dependence of their solutions on the right hand-hand side. The latter depends itself continuously on the data set \mathbb{X} because the Dirac distribution δ_x depends continuously on its location $x \in \mathbb{R}^d$ in the topology of $H^{-\frac{d+1}{2}}(\mathbb{R}^d)$ as follows from the Sobolev embedding

$$\|\delta_x - \delta_{\tilde{x}}\|_{H^{-\frac{d+1}{2}}} = \sup_{\|\varphi\|_{H^{\frac{d+1}{2}}} = 1} |\langle \delta_x - \delta_{\tilde{x}}, \varphi \rangle| = \sup_{\|\varphi\|_{H^{\frac{d+1}{2}}} = 1} |\varphi(x) - \varphi(\tilde{x})| \leq C |x - \tilde{x}|^{\frac{1}{2}}, \quad x, \tilde{x} \in \mathbb{R}^d$$

thanks to $\sup_{x \neq \tilde{x}} \frac{|\varphi(x) - \varphi(\tilde{x})|}{|x - \tilde{x}|^{1/2}} \leq C \|\varphi\|_{H^{\frac{d+1}{2}}}$ and because the values of $u_{\mathbb{X}}$ on \mathbb{X} are obtained from a linear system, the matrix of which depends continuously on \mathbb{X} as well. A similar reasoning can be applied when the chosen kernel is Gaussian. In that case, we use the continuous dependence of the solution of the heat equation on its initial data in the weak norm and the regularizing effect of the heat equation

for positive times. The initial data are again a finite linear combination of Dirac distributions supported on the data set, the coefficients of which also depend continuously on the data set. \square

Remark 3.2. *Thinking of equations (3.2) & (3.3) as discretizations of equations (2.7) & (2.11) and equations (2.9) & (2.13) (depending on the choice of kernel), it would appear, that that weight of the surface measure $d\sigma_{\mathcal{M}}$ has been neglected (and it has), but since the focus is on the signature function $u_{\mathbb{X}}$, there is no need to have direct access to it and we can think of it as being incorporated in the density function Λ_m^α .*

Remark 3.3. *Interpreting equations (3.2) & (3.3) as discretization of their continuous counterpart is useful for the structural understanding of the problem. It is, however, remarkable that the solutions $u_{\mathbb{X}}$ produced by equations (3.2) & (3.3) are themselves minimizers of an infinite dimensional optimization problem. Take the Laplace kernel case, for instance. Then $u_{\mathbb{X}}$ is the minimizer of the energy*

$$E_{\alpha, \mathbb{X}}(u) = E_0(u) + \frac{1}{2\alpha m} \sum_{i=1}^m |u(x^i) - 1|^2,$$

with the understanding that the second term is replaced by the constraint $u|_{\mathbb{X}} \equiv 1$ when $\alpha = 0$. This optimization problem is well-defined for any data set \mathbb{X} since $H^{\frac{d+1}{2}}(\mathbb{R}^d) \hookrightarrow BUC(\mathbb{R}^d)$. It was computed in [10] for $\alpha > 0$ that the corresponding Euler-Lagrange equation is given by

$$\alpha Au = \frac{1}{m} \sum_{i=1}^m [1 - u(x^i)] \delta_{x^i}.$$

This connection also explains the efficacy of the use of the level sets of $u_{\mathbb{X}}$ for classification purposes demonstrated in [10]. A similar discussion applies in the case of the Gauss kernel. Indeed, the function

$$\frac{1}{m} \sum_{k=1}^m e^{-|x-x_k|^2} \Lambda_m^k$$

is the solution of the heat equation evaluated at time $t = \frac{1}{4}$ with initial datum

$$\frac{\pi^{d/2}}{m} \sum_{k=1}^m \Lambda_m^k \delta_{x^k},$$

thus yielding a direct interpretation of equation (3.2) (and similarly of equation (3.3)) when $K = G$.

Remark 3.4. *As a matter of fact, the discrete case can be subsumed to the general case by simply setting $\mathcal{M} = \mathbb{X}$ and setting*

$$\delta_{\mathcal{M}} = \delta_{\mathbb{X}} := \frac{1}{m} \sum_{i=1}^m \delta_{x^i}.$$

When \mathbb{X} is used or thought of as an approximation of a continuous manifold \mathcal{M} , however, this interpretation is not always fully compatible with convergence as the discrete points “fill” the manifold \mathcal{M} as explained above.

Remark 3.5. *We point out that equations like (3.2) and (3.3) written as*

$$M\Lambda = m\mathbf{1}_m \text{ and } (m\alpha + M)\Lambda = m\mathbf{1}_m$$

respectively, arise and have been extensively studied and used for interpolation and statistical purposes for general right-hand side (above $\mathbf{1}_m$ denotes the vector of length m with all components 1). The first as the natural equation for the computation of an interpolant via the method of Reproducing Kernel Hilbert Spaces [27], and the second as a Ridge Regression in statistics [26]. In the context of point clouds [5] and the implicit representation of hypersurfaces, it appears customary to find local neighborhoods and use methods like principal component analysis to obtain an approximate tangent plane (and normal vector) in order to construct a defining function by prescribing its values at off-surface points. This

approach, often based on the identification of k nearest neighbors and principal component analysis, is described e.g. in [27] as an application of meshless interpolation methods. The framework developed here, shows how kernel methods of the kind discussed in [27] can, in fact, give direct access to the geometry of the surface simply using a (not necessarily ordered) sample of the points on (or near) it. For a more thorough discussion of these connections we refer to [11].

Remark 3.6. While we will not pursue this angle in this paper further, we point out that the proposed approach, while global in nature, can be modulated to possess varying degrees of non-locality. The kernel K can indeed be replaced by $K(\delta \cdot)$ for $\delta > 0$, which determines the width of its bump.

4. SYMMETRIES

In this short section we mainly remark that the signature function $u_{\mathcal{M}}$ inherits any symmetries enjoyed by the manifold \mathcal{M} .

Proposition 4.1. *Let $R : \mathbb{R}^d \rightarrow \mathbb{R}^d$ be any rigid transformation with the property that $R(\mathcal{M}) = \mathcal{M}$. Then it holds that*

$$u_{\mathcal{M}}(R \cdot) = u_{\mathcal{M}}.$$

Proof. For the Laplace case, notice that the energy functional E_0 satisfies $E_0(u) = E_0(u \circ R)$ so that u and $u \circ R$ are both minimizers since they both satisfy the constraint (which is also invariant under any self-map of \mathcal{M}). Uniqueness then implies that they coincide. When $\alpha > 0$, the additional term in the functional satisfies

$$\mathcal{f}_{\mathcal{M}} f(Rx) d\sigma_{\mathcal{M}}(x) = \mathcal{f}_{R^{-1}\mathcal{M}} f(Rx) d\sigma_{\mathcal{M}}(Rx) = \mathcal{f}_{\mathcal{M}} f(x) d\sigma_{\mathcal{M}}(x),$$

for any $f \in L^1(\mathcal{M})$ since $\mathcal{M} = R^{-1}\mathcal{M}$ and $R_*\sigma_{\mathcal{M}} = \sigma_{\mathcal{M}}$ by assumption, where here and below R^* and R_* are the pull-back and push-forward by R , respectively. For the Gaussian case, notice that equation (2.13) is invariant with respect to R

$$\mathbf{1}_{\mathcal{M}} = R_*\mathbf{1}_{\mathcal{M}} = R_*((\alpha + \mathcal{G})\Lambda) = R_*(\alpha + \mathcal{G})R^*R_*\Lambda = (\alpha + \mathcal{G})R_*\Lambda,$$

since

$$\mathcal{f}_{\mathcal{M}} e^{-|Rx-z|^2} f(R^{-1}z) d\sigma_{\mathcal{M}}(z) = \mathcal{f}_{R^{-1}\mathcal{M}} e^{-|Rx-Ry|^2} f(y) d\sigma_{\mathcal{M}}(Ry) = \mathcal{f}_{\mathcal{M}} e^{-|x-y|^2} f(y) d\sigma_{\mathcal{M}}(y).$$

Uniqueness again yields the claim together with the fact that the restriction of the signature function to \mathcal{M} is directly related to the density Λ^α in the Gaussian case via

$$u_{\mathcal{M}}^\alpha|_{\mathcal{M}} = 1 - \alpha\Lambda^\alpha,$$

just as in the Laplace case, a fact which was noted in Proposition 2.5. When the data set \mathbb{X} enjoys a symmetry, it will therefore be reflected in its signature function $u_{\mathbb{X}}$. \square

When the data set is a sample of a continuous manifold, the symmetry properties of the manifold will be approximately reflected in the signature function of the sample, as well. This is apparent in some of the experiments considered in the last section. As already mentioned in passing above, in some cases the signature function is not a regular defining function in the sense that the value 1 is not a regular value for it. This happens when the manifold is flat, for instance. A simple example is given by the real line $\mathbb{R} \times \{0\} \subset \mathbb{R}^d$ for which, taking $\alpha = 0$ and using the Gaussian kernel we see that

$$\int_{-\infty}^{\infty} e^{-|x_1-y_1|^2 - |x'|^2} \Lambda(y_1) dy_1 = e^{-|x'|^2} \int_{-\infty}^{\infty} e^{-|x_1-y_1|^2} \Lambda(y_1) dy_1,$$

where $x' = (x_2, \dots, x_d)$. We know that the signature function and hence the density Λ is translation invariant and hence constant on the real line so that

$$\Lambda = \left(\int_{-\infty}^{\infty} e^{-|x_1-y_1|^2} dy_1 \right)^{-1} = \left(\int_{-\infty}^{\infty} e^{-y_1^2} dy_1 \right)^{-1}.$$

Then 1 is not a regular value of $u_{\mathcal{M}} = e^{-|x'|^2}$. It is, however, possible to compute normals by moving even only slightly away from the line at any point of interest along it. In general, the presence of curvature will ensure that this does not happen as values on one side of a hypersurface will be higher than on the other as would be the case in the example, if the line were bent and $d = 2$. The example of the line also shows how the signature function of a manifold falls off rapidly and generates rapidly turning normals in any direction that is not tangent to it. This will be exploited in order to estimate the local dimension of a manifold from its samples.

5. THE GEOMETRY OF POINT CLOUDS

In this section we use the signature functions obtained in the previous sections to analyze the normal and the curvature of manifolds sampled at finitely many points. If the starting point is a point cloud, then its signature function yields an interpolated continuous manifold of which geometric quantities can be computed and used to understand the point cloud itself. The idea is straightforward: if the point cloud is known or for some reason supposed to be “smooth”, then the use of the Gauss kernel is most appropriate, while, in cases where the surface is known to possess only low regularity, the best choice is the Laplace kernel. This point will be further discussed in the next section, where the noisy situation is considered as well and regularization plays an even more important role. We discuss the approach for the case of hypersurfaces and for the Gauss kernel first because of its higher degree of smoothness. Given a point cloud \mathbb{X} of size m , we compute the associate density function $\Lambda_m^\alpha \in \mathbb{R}^m$ by solving equation (3.3) and obtain

$$u_{\mathbb{X}}(x) = \frac{1}{m} \sum_{j=1}^m \lambda_j e^{-|x-x^j|^2}, \quad x \in \mathbb{R}^d,$$

where, from now on, we set $\lambda_j = \Lambda_m^{\alpha,j}$ for simplicity of notation. Then we compute the normal $\nu_{\mathbb{X}}$ as

$$\nu_{\mathbb{X}} = -\frac{\nabla u_{\mathbb{X}}}{|\nabla u_{\mathbb{X}}|},$$

which is of particular interest at $x \in \mathbb{X}$, where

$$\nabla u_{\mathbb{X}}(x) = -2 \sum_{j=1}^m \lambda_j e^{-|x-x^j|^2} (x - x^j), \quad x \in \mathbb{R}^d$$

and where the sign is chosen in order to obtain the outer unit normal in the case of a unit circle. Next we compute the Hessian of $u_{\mathbb{X}}$

$$[D^2 u_{\mathbb{X}}]_{kl} = 4 \sum_{j=1}^m \lambda_j e^{-|x-x^j|^2} (x_k - x_k^j)(x_l - x_l^j) - 2\delta_{kl} \sum_{j=1}^m \lambda_j e^{-|x-x^j|^2},$$

from which a direct calculation yields the Jacobian of $\nu_{\mathbb{X}}$

$$D\nu_{\mathbb{X}} = \frac{1}{|\nabla u_{\mathbb{X}}|} (D^2 u_{\mathbb{X}} - D^2 u_{\mathbb{X}} \nu_{\mathbb{X}} \nu_{\mathbb{X}}^T).$$

Now $\nu_{\mathbb{X}}$ is clearly an eigenvector of $D\nu_{\mathbb{X}}$ to the eigenvalue 0, while the other eigenvalues are the principal curvatures of the surface. Points at which $u_{\mathbb{X}}$ is not a regular defining function, i.e. at which $\nabla u_{\mathbb{X}}$ vanishes, cannot be excluded but a small perturbation can be applied numerically to still obtain a meaningful approximation and avoid the singularity as discussed previously. When the point cloud represents a full measure or open subset of the ambient space, the signature function is better thought of a smooth approximation of its characteristic function. When the codimension is higher than one, the method still computes a normal to the interpolated manifold and its curvatures. The latter are, however, found along with spurious curvatures due to the fact that the method always generates hypersurfaces for most of its level sets. In the case of the real line in higher dimensional space, it follows from the example at the end of the previous section that most level sets are cylinders.

The Laplace kernel would appear not to be a viable option for the computation of normals and curvatures due to its lack of smoothness. In practice, however, it is sufficient to use a slight regularization of the kernel given by

$$L_r(x) = e^{-\sqrt{|x|^2+r}}, x \in \mathbb{R}^d,$$

for $r > 0$ small, which leads to the well-defined expressions

$$\partial_j L_r(x) = -e^{-\sqrt{|x|^2+r}} \frac{x^j}{\sqrt{|x|^2+r}}, x \in \mathbb{R}^d, j = 1, \dots, d$$

and

$$\partial_i \partial_j L_r(x) = e^{-\sqrt{|x|^2+r}} \left(\frac{x^i x^j}{|x|^2+r} + \frac{\delta_{ij}}{\sqrt{|x|^2+r}} - \frac{x^i x^j}{(|x|^2+r)^{3/2}} \right), x \in \mathbb{R}^d, i, j = 1, \dots, d,$$

that can be used as in the calculations described above for the case of the Gauss kernel. This approach consistently yields good estimates for the normal and, when the data set is dense enough (denser than the scale determined by $r > 0$), also computes viable curvature approximations.

Remark 5.1. *It is important to stress the fact that this approach does not require any organization of the points in the point cloud. The use of the kernel implicitly takes advantage of local neighborhoods while maintaining a global significance by including the influence of every single point in the cloud.*

Remark 5.2. *The simplest point cloud consists of a single point $x_0 \in \mathbb{R}^d$, in which case $u_{\mathbb{X}}$ yields a function peaked at x_0 and possessing spheres centered at x_0 as its level sets (regardless of the choice of kernel). In the general case, these building blocks combine in a way determined by the geometry of the point cloud and the underlying PDE to yield a meaningful signature function.*

Remark 5.3. *The regularization approach described above for the Laplace kernel will be followed in the numerical implementation of the experiments performed in the next section.*

6. NUMERICAL EXPERIMENTS

In this section we demonstrate how the two “extremal” methods described in the previous sections can be successfully used for the purposes described and highlight their distinct specific behaviors and advantages.

6.1. A Circle. First we consider an analytic curve, the unit circle. We present the results of experiments using 30 regularly spaced points along the circle performed with both the Gaussian and the Laplace kernel without noise as well as with various degrees of noise for several values of the regularization parameter α . In the noisy experiments, the percent is of the maximal distance between consecutive points. In this way, the noise level depends only on the data itself but can be related to the discretization level if the data set represents a sample of points on the circle. The noise itself is uniform in direction and in size. Figure 6.1.1 depicts the implied level line (in red) and the implied normals. The latter are evaluated at the given points but, clearly, could be evaluated anywhere. The level lines are computed by evaluating the data signature function on a regular grid of a surrounding box. There is no discernible difference between the two regularization levels, $\alpha = 0, 10^{-10}$ in this smooth example with exact data. We shall see later that the curvature is accurately captured with the Gauss kernel, while it is not, for this coarse grid, for the Laplace kernel. The use of regularization, however, limits the achievable accuracy as reflected in an upcoming numerical estimation of curvature below. It can be seen in the images of Figure 6.1.1 that the signature function’s level set (in red) has sharp corners at the data points when using the Laplace kernel. Away from the data, the level sets are smooth and reflect the symmetry properties of the point cloud.

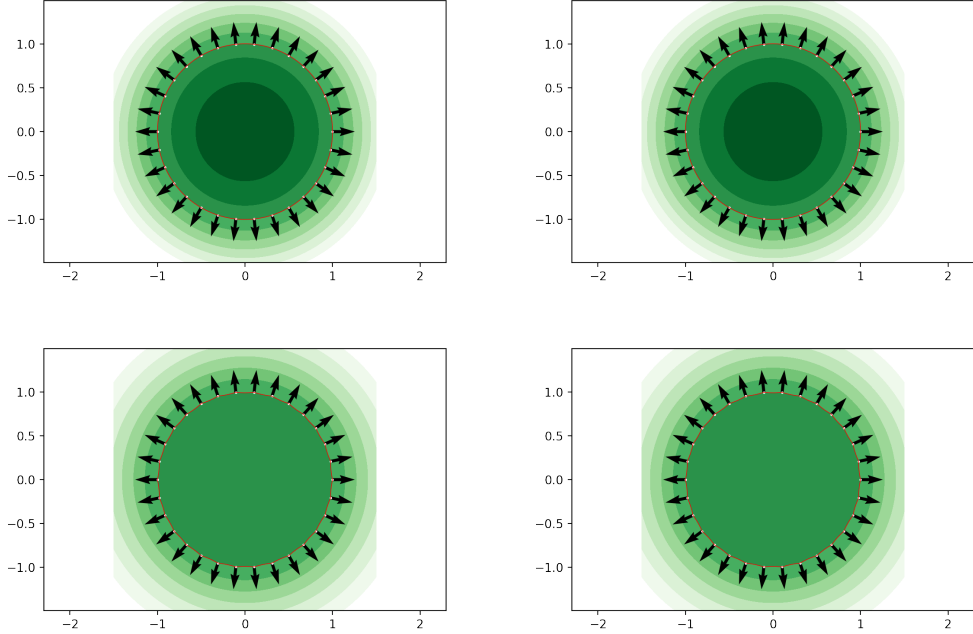


FIGURE 6.1.1. The top row depicts level lines of the signature function of the 30 white points and the implied normals obtained using the Gaussian kernel. The second row depicts the same for the Laplace kernel. The experiments in the first column correspond to no regularization ($\alpha = 0$), whereas $\alpha = 10^{-10}$ for the ones in the right column.

6.2. A Square. Next we consider a non-smooth curve, the boundary of a square. This example shows how the Laplace kernel can more closely follow the boundary as it generates a solution of a PDE that is merely (Hölder) continuous. It is interesting to observe how the level lines of the signature function obtained with the Gauss kernel can also reproduce the square but since the signature function is analytic it does so by splitting the whole curve into two smooth closed curves[‡], of which union the square is a part of. We shall soon see that this does not prevent the use of the Gauss kernel in more general circumstances but leads to the need of using some regularization to control the shape of the level lines. Again it is apparent how the level lines smooth out and simplify away from the non-smooth curve considered.

6.3. A sector. In Table 6.3.1 we compute the error between the exact and implied curvatures for a sector of a unit circle of angle $\frac{\pi}{16}$ for both the Gauss and Laplace kernels. It shows the high accuracy achieved with relatively few points by the Gauss kernel. It also showcases the ability of the (regularized) Laplace kernel to obtain a good approximation. We restrict the error analysis to the middle quarter of the sector since the accuracy naturally deteriorates in the regions around the end points. It is also apparent that the accuracy of the unregularized Gauss kernel saturates (due to the increasing ill-conditioning of the discrete system), while regularization is essentially unnecessary for the Laplace kernel, again due to the fact that the discrete system corresponds to a differential operator of “minimal order” and leads to significantly less ill-conditioning.

[‡]This is the reason why the normal points into the square in this case

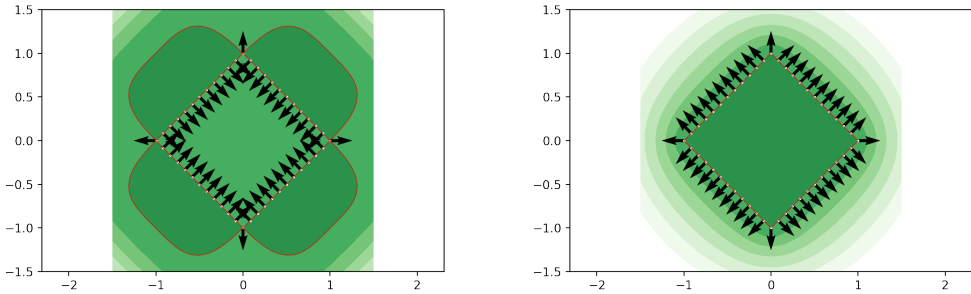


FIGURE 6.2.1. The level lines of the signature function of the 48 white points and the implied normals obtained using the Gaussian kernel (left) and Laplace Kernel (right). We used $\alpha = 10^{-10}$ for both.

Method/Points		32	64	128	256
Gauss	$\alpha = 0$	2.26×10^{-6}	2.16×10^{-6}	1.54×10^{-6}	5.51×10^{-6}
	$\alpha = 10^{-10}$	5.47×10^{-4}	2.78×10^{-4}	1.24×10^{-4}	4.22×10^{-5}
Laplace	$\alpha = 0$	4.84	0.24	5.12×10^{-4}	1.01×10^{-6}
	$\alpha = 10^{-10}$	4.84	0.24	5.12×10^{-4}	7.55×10^{-7}

TABLE 6.3.1. The average relative error between the exact and the implied curvature at the points found in the middle quarter of a sector of the unit circle of aperture $\frac{\pi}{16}$.

The experiments considered so far show the respective benefits of the two kernels. The Gauss kernel delivers an analytic signature which attempts to place the data points on a union of smooth curves, while the Laplace kernel leads to a merely continuous signature which can therefore exhibit level sets that more closely follow the data points, even as they go through corners (singularities in general).

6.4. Noisy Circle and Square. The benefits just discussed are even more evident in the experiments depicted in Figures 6.4.1-6.4.3 and 6.4.4-6.4.5, where the data points are randomly displaced from their original position along the circle and along the boundary of the square. The new points are obtained from the old ones by adding a displacement of 5% and 50% which is uniform in direction and in distance. The percentage refers to maximal displacement size as a fraction of the maximal distance between consecutive data points. In this way, the error is directly related to the data set, which is in general all that is available. Notice, however, that the ordering (parametrization) of the points is not in any way required knowledge for the construction of the signature function. Figure 6.4.2 shows the realization of the random data sets with different levels of noise for the experiments depicted in Figures 6.4.1-6.4.3 and 6.4.4-6.4.5 obtained by the use of the Gaussian kernel. The corresponding experiments with the Laplace kernel are based on a different realization of the perturbed data set that is not depicted in this paper. It is evident how the analytic signature tries to accommodate smooth level lines through the data without necessarily connecting the points in what the human eye would consider the natural way. Notice, however, how the implied normals can still approximately capture the tangent line to the “average curve”. The introduction of regularization, by allowing for approximate interpolation, makes it possible for the method to successfully connect the dots into a smooth line and

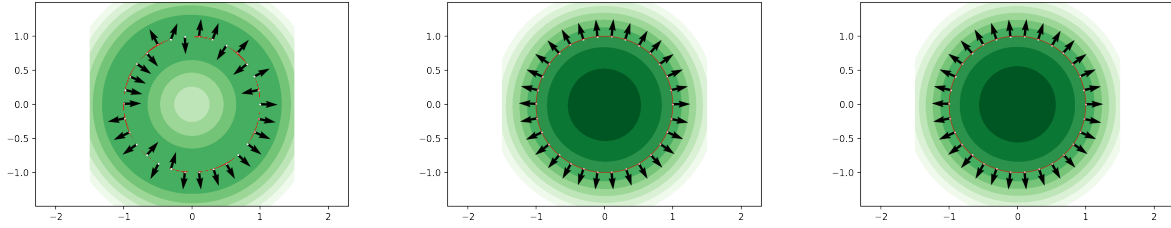


FIGURE 6.4.1. The circle example revisited by randomly displacing the original exact sample by 5% noise. Depicted are the level lines and implied normals obtained by means of the Gauss kernel based signature function computed with different regularization levels $\alpha = 0, .01, .1$ in increasing order from left to right.

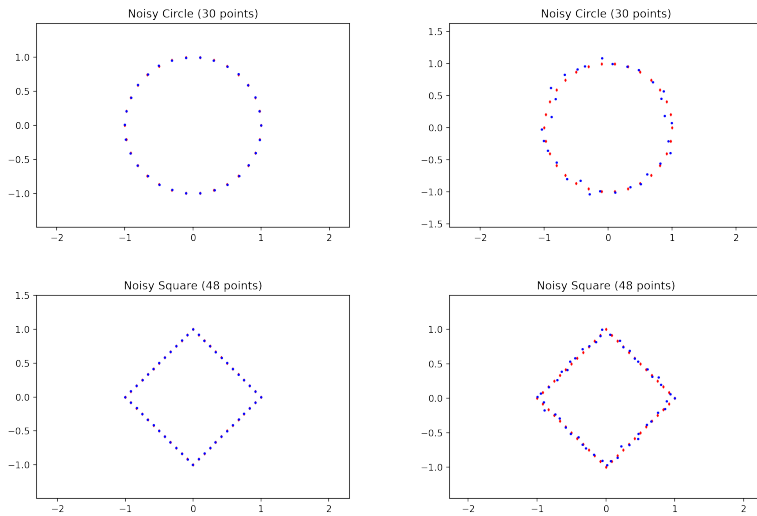


FIGURE 6.4.2. The original set of data points is shown in all images as red diamonds. The blue dots show the noise-perturbed data points at the different noise levels: 5% and 50% from left to right.

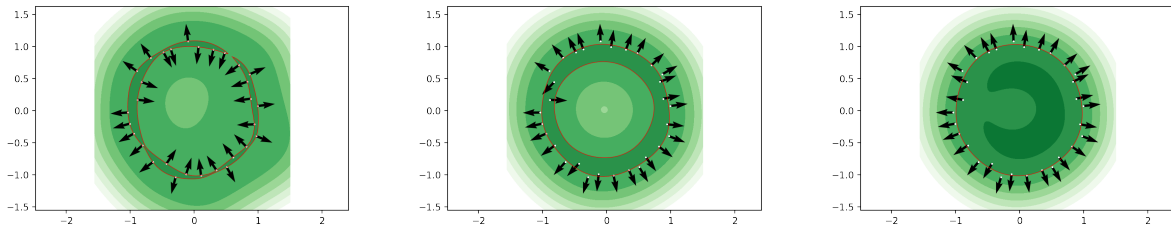


FIGURE 6.4.3. The circle example revisited by randomly displacing the original exact sample by 50% noise. Depicted are the level lines and implied normals obtained by means of the Gauss kernel based signature function compute with different regularization levels $\alpha = 0, .01, .1$ in increasing order from left to right.

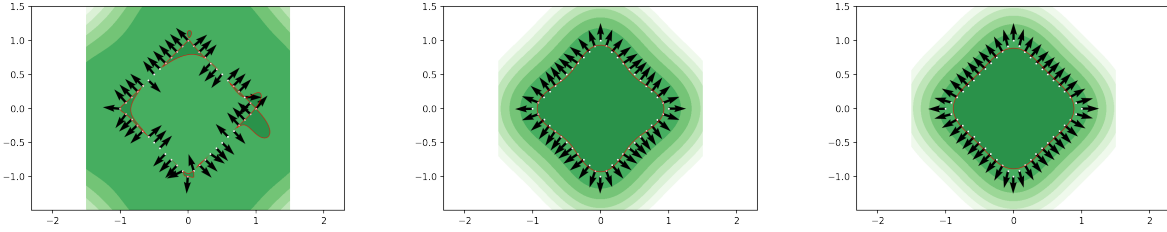


FIGURE 6.4.4. The square example revisited by randomly displacing the original exact sample by 5% noise. Depicted are the level lines and implied normals obtained by means of the Gauss kernel based signature function computed with different regularization levels $\alpha = 0, .01, .1$ in increasing order from left to right.

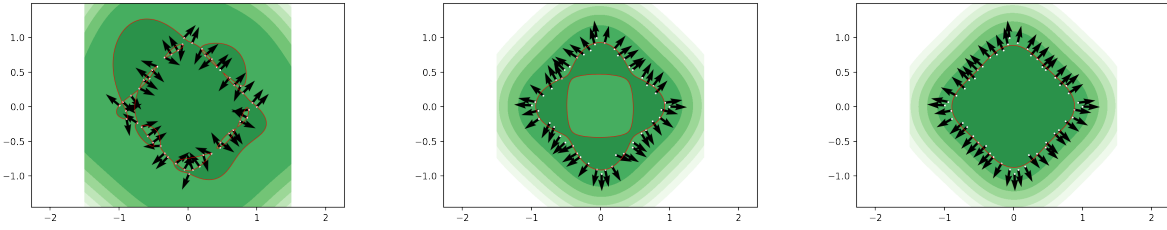


FIGURE 6.4.5. The square example revisited by randomly displacing the original exact sample by 50% noise. Depicted are the level lines and implied normals obtained by means of the Gauss kernel based signature function computed with different regularization levels $\alpha = 0.01, .1$ in increasing order from left to right

capture its normal vector. In these and subsequent numerical experiments, the level line depicted in red is that corresponding to the average value of the signature function on the data set.

6.5. A Graph. The experiments found in Figures 6.5.1 and 6.5.2 show the method applied to a non-smooth graph locally around the origin without and with noise. In Tables 6.5.1-6.5.2 we record the implied normals and curvatures computed at the origin with the Gauss kernel at various regularization and noise levels. Again the normal appears to be computed in a very stable manner across noise and regularization levels.

Noise/Regularization	0	10^{-10}	.01	.05	.1
0%	(-.000002, 1.)	(0., -1.)			
5%	(0.0568, -0.998)	(0.0025, -1.)	(-.000419, -1.)	(-.000368, -1.)	(-.000407, -1.)
10%	(.000892, 1.)	(-0.0152, -0.9999)	(.000821, -1.)	(.000332, -1.)	(.000835, -1.)
50%	(0.016, 1.)	(0.0885, 0.996)	(0.0031 - 1.)	(-.000419, -1.)	(-0.00364, -1.)

TABLE 6.5.1. Implied normal at the origin for the graph experiment.

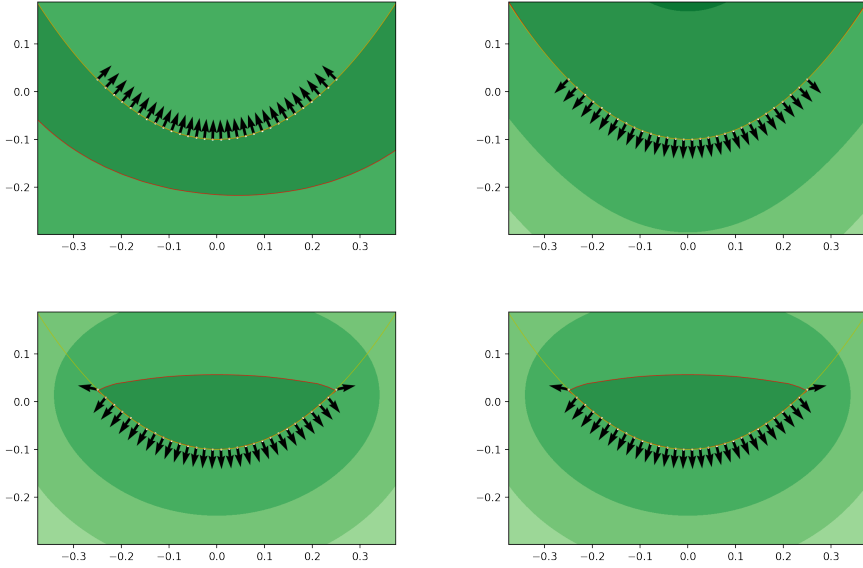


FIGURE 6.5.1. The top row depicts the implied level line (in red) of the signature function of the graph (in yellow) of the function $y = -1 + x^2 + |x|^{2.5}$ for $x \in [-.25, .25]$ along with the implied normals (at the data points) obtained using the Gaussian kernel. The second row depicts the same for the Laplace kernel. The experiments in the first column correspond to no regularization ($\alpha = 0$), where $\alpha = 10^{-10}$ for the ones in the right column.

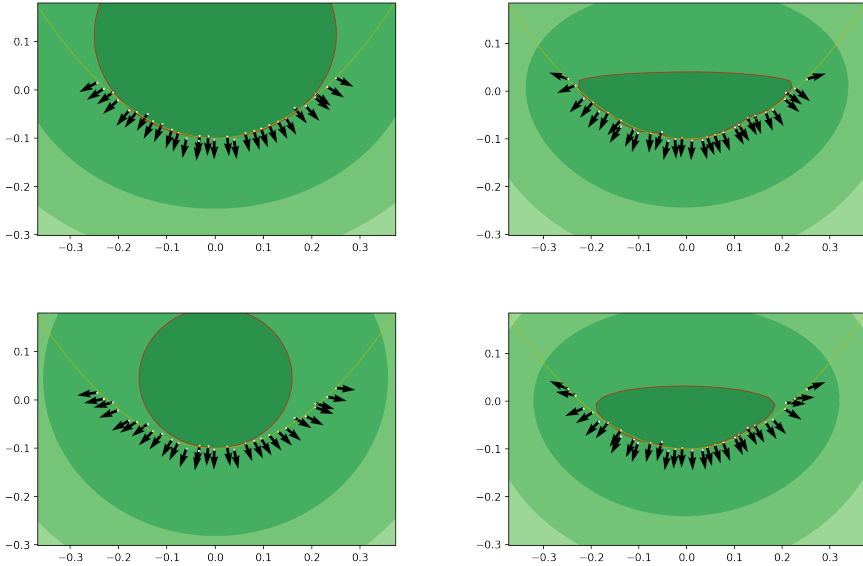


FIGURE 6.5.2. The graph example revisited by randomly displacing the original exact sample by 50% noise. Depicted are the level lines and implied normals obtained by means of the Gauss (left column) and Laplace (right column) kernel based signature function computed with different regularization levels $\alpha = .01, .1$ in increasing order from top left to bottom right.

Noise/Regularization	0	10^{-10}	.01	.05	.1
0%	-4.	3.999			
5%	40.10	3.0307	3.301	4.410	5.6205
10%	-4935	3.295	3.3	4.412	5.6385
50%	-0.9671	-10.52	3.359	4.513	5.764

TABLE 6.5.2. Implied curvature at the origin for the graph experiment.

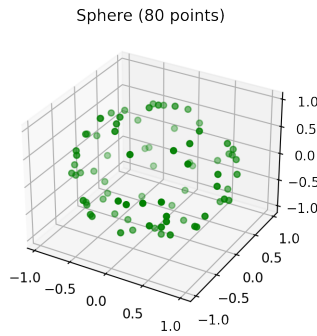


FIGURE 6.6.1. 80 points randomly sampled from the unit sphere.

6.6. A Sphere. Next we consider an example where $d = 3$, starting with the unit sphere. We take a random sample of points of size $m = 80$ that lie exactly on the sphere and used them to compute the signature function, which, in turn, we use to obtain the implied curvature at another set of randomly chosen points on the sphere. The random sample is generated by choosing x_3 uniformly at random from $[-1, 1]$ and then setting $x = (\sqrt{1 - x_3^2} \cos(\theta), \sqrt{1 - x_3^2} \sin(\theta), x_3)$ for θ uniformly distributed in $[0, 2\pi)$. It is depicted in Figure 6.6.1. Then we evaluate the signature function and compute the implied normals and implied curvatures at 32 other points on the sphere sampled in the same way. The maximum deviation from the value 1 of the signature function at these points is .0000225, the maximum angle between the exact normal and the implied normal is 0.00873 degrees, and the maximum error in curvature is 0.0143.

6.7. A Folded Shape. Finally we consider an example where approaches to manifold learning or reconstruction via local neighborhoods could lead to erroneous results unless a dense enough sample is used for the manifold along with a carefully chosen neighborhood size. We consider a closed curve obtained as the combination of segments and semicircles discretized at a level where nearby points in the ambient space can be far from each other if the distance is measured on the manifold. The shape is the one implied by its discrete sample in Figure 6.7.1 (left) and its accurate interpolation (red line). The method is clearly able to connect the dots in the proper way. Notice that, while this is true for closed compact manifolds, this is no longer the case if the manifold has boundary as Figure 6.7.1 (right) clearly shows (at least at this level of discretization). The curve on the right is obtained by removing the obvious part of the closed curve. In this example we used the regularized ($r = 1$) Laplace kernel with $\alpha = 10^{-10}$.

6.8. Dimension Estimation. We use the closed curve C above and the surface S obtained by replacing each point $(x, 0, z)$ on the curve with the segment $\{x\} \times [-.5, .5] \times \{z\}$. While S is a surface

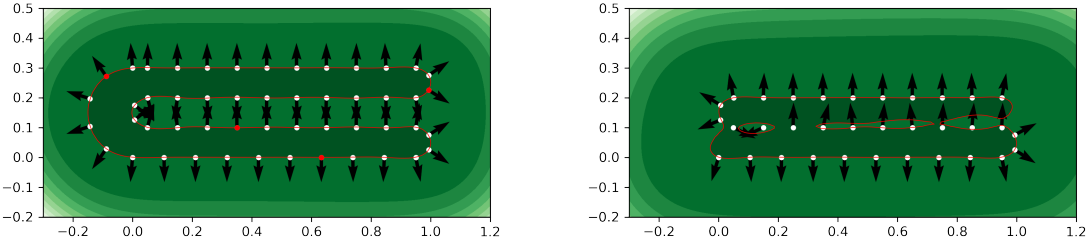


FIGURE 6.7.1. This example illustrates how the method can connect the dots properly for closed manifolds (left) even when other methods based on local neighborhoods struggle due to limited sample density. This is not true for manifolds with boundary (right), at least when the sampling density is insufficient. Some of the points in the left cloud are red for reasons related to the experiment discussed in the next subsection.

with boundary, we shall take samples where $y = 0$, i.e. away from the boundary. The idea is to exploit the fact that the signature function of the curve C viewed as a subset of \mathbb{R}^3 contained in $\mathbb{R} \times \{0\} \times \mathbb{R}$ reproduces this curve as a limit of the two dimensional surface $[u_C = 1 - \varepsilon]$ which wraps around the curve. The sections of this surfaces in the orthogonal plane to any point along the curve are small ‘‘circles’’ (circles exactly if the curve were a straight line as shown at the end of Section 4). As a consequence, the normal to these surfaces turns very quickly in the vicinity of points on the curve. On the other hand the normal to the surface S does not turn locally (in a neighborhood the size of which depends on the local curvature) nearly as much since S is well approximated by its tangent plane that is also slowly varying across nearby level sets. We therefore take a sample of points in the immediate vicinity of the point of interest (from the data set) and use the corresponding signature functions u_C and u_S to compute the implied normals (to the associated level set surfaces) at these points. The (numerical) rank r of the matrix obtained by using the computed normals as columns provides a way to estimate the local dimension. The dimension of the tangent space to the implied hypersurface is clearly $d - 1 = 2$ in both cases but, for directions in the orthogonal space of the actual manifold, the quick turning will generate linearly independent vectors, while in tangential directions, the normals will point in similar directions. This works for submanifolds of any dimension and produces an estimate for the dimension given by $d - r$.

Table 6.8.1 below shows the singular values obtained along the central curve C (corresponding to the red data points in the two dimensional projection of Figure 6.7.1) based on u_C and on u_S . The points are ordered left to right, bottom to top. The first set is for the curve, whereas the second is for the surface. Shown are the singular values of a 3×15 matrix generated by taking the implied normals computed at 15 random perturbations of the points as its columns. The perturbation consists in translating the point in a random direction to a point at a random distance uniformly distributed in $[0, 0.01]$. The numerical rank is clearly 2 for the points on the curve, whereas it is 1 for same points on the surface. Thus the numerically estimated local dimension at the chosen points is 1 for the curve and 2 for the surface.

REFERENCES

- [1] R. A. Adams. *Sobolev Spaces*. Academic Press, New York, 1975.
- [2] Mikhail Belkin and Partha Niyogi. Laplacian eigenmaps for dimensionality reduction and data representation. *Neural Computation*, 15(6):1373–1396, 2003.

	sv1	sv2	sv3	sv1	sv2	sv3
Point 1	3.25	2.11	8.78×10^{-4}	3.87	1.46×10^{-2}	4.02×10^{-4}
Point 2	3.42	1.81	2.45×10^{-3}	3.87	5.34×10^{-3}	4.44×10^{-3}
Point 3	3.28	2.05	8.39×10^{-2}	3.87	2.18×10^{-1}	1.66×10^{-3}
Point 4	3.03	2.41	8.62×10^{-2}	3.87	9.94×10^{-2}	9.07×10^{-5}

TABLE 6.8.1. Estimation of the local dimension based on the rank of the span of implied normals at randomly chosen points in the immediate vicinity of selected data points.

- [3] Mikhail Belkin and Partha Niyogi. Towards a theoretical foundation for laplacian-based manifold methods. *Journal of Computer and System Sciences*, 74(8):1289–1308, 2008.
- [4] Yoshua Bengio, Jean-François Paiement, Pascal Vincent, Olivier Delalleau, Nicolas Roux, and Marie Ouimet. Out-of-sample extensions for lle, isomap, mds, eigenmaps, and spectral clustering. *Advances in Neural Information Processing Systems*, 16:177–184, 2004.
- [5] Matthew Berger, Andrea Tagliasacchi, Lee M. Seversky, Pierre Alliez, Gaël Guennebaud, Joshua A. Levine, Andrei Sharf, and Claudio T. Silva. A survey of surface reconstruction from point clouds. *Computer Graphics Forum*, 36(1):301–329, 2017.
- [6] Ronald R Coifman, Ioannis G Kevrekidis, Stéphane Lafon, Mauro Maggioni, and Boaz Nadler. Diffusion maps, spectral clustering and reaction coordinates of dynamical systems. *Applied and Computational Harmonic Analysis*, 21(1):113–127, 2006.
- [7] Ronald R Coifman and Stéphane Lafon. Diffusion maps. *Applied and Computational Harmonic Analysis*, 21(1):5–30, 2006.
- [8] Ronald R Coifman, Stéphane Lafon, Ann B Lee, Mauro Maggioni, Boaz Nadler, Frederick Warner, and Steven W Zucker. Geometric diffusions as a tool for harmonic analysis and structure definition of data: Diffusion maps. *Proceedings of the National Academy of Sciences*, 102(21):7426–7431, 2005.
- [9] John C. Gower. Some distance properties of latent root and vector methods used in multivariate analysis. *Biometrika*, 53(3-4):325–338, 1966.
- [10] P. Guidotti. Dimension Independent Data Sets Approximation and Applications to Classification. *Advanced Modeling and Simulation in Engineering Sciences*, 11(1), 2024.
- [11] P. Guidotti. Geometric kernel interpolation and regression. *arXiv preprint*, 2026.
- [12] Matthias Hein, Jean-Yves Audibert, and Ulrike von Luxburg. Graph laplacians and their convergence on random neighborhood graphs. *Journal of Machine Learning Research*, 8:1325–1368, 2007.
- [13] Harold Hotelling. Analysis of a complex of statistical variables into principal components. *Journal of Educational Psychology*, 24(6):417–441, 1933.
- [14] P. W. Jones, M. Maggioni, and R. Schul. Universal local parametrizations via heat kernels and eigenfunctions of the laplacian. *Ann. Acad. Sci. Fenn. Math.*, 35:131–174, 2010.
- [15] Dhruv Kohli, Alexander Cloninger, and Gal Mishne. Ldle: Low distortion local eigenmaps. *Journal of Machine Learning Research*, 22(282):1–64, 2021.
- [16] Dhruv Kohli, Sawyer J. Robertson, Gal Mishne, and Alexander Cloninger. Robust tangent space estimation via laplacian eigenvector gradient orthogonalization, 2025.
- [17] Stéphane Lafon and Ann B Lee. Diffusion maps and coarse-graining: A unified framework for dimensionality reduction, graph partitioning, and data set parameterization. *IEEE Transactions on Pattern Analysis and Machine Intelligence*, 28(9):1393–1403, 2006.
- [18] T. Leinster. The Euler characteristic of a category. *Documenta Mathematica*, 13:21–49, 2008.
- [19] T. Leinster. The magnitude of metric spaces. *Documenta Mathematica*, 18:857–905, 2013.
- [20] T. Leinster. The magnitude of a graph. *Mathematical Proceedings of the Cambridge Philosophical Society*, 166(2):247–264, 2019.
- [21] T. Leinster and S. Willerton. On the asymptotic magnitude of metric spaces. *Geometriae Dedicata*, 164(1):287–310, 2013.
- [22] Mark W. Meckes. Positive definite metric spaces. *Positivity*, 17:733–757, 2013.
- [23] Karl Pearson. On lines and planes of closest fit to systems of points in space. *The London, Edinburgh, and Dublin Philosophical Magazine and Journal of Science*, 2(11):559–572, 1901.
- [24] Joshua B. Tenenbaum, Vin de Silva, and John C. Langford. A global geometric framework for nonlinear dimensionality reduction. *Science*, 290(5500):2319–2323, 2000.

- [25] Warren S. Torgerson. Multidimensional Scaling: I. Theory and Method. *Psychometrika*, 17(4):401–419, 1952.
- [26] Grace Wahba. *Spline Models for Observational Data*, volume 59 of *CBMS-NSF Regional Conference Series in Applied Mathematics*. Society for Industrial and Applied Mathematics, Philadelphia, PA, 1990.
- [27] H. Wendland. *Scattered Data Approximations*. Number 17 in Cambridge Monographs on Applied and Computational Mathematics. Cambridge University Press, Cambridge, 2004.
- [28] Holger Wendland. Fast evaluation of radial basis functions: methods based on partition of unity. In *Approximation Theory X: Wavelets, Splines, and Applications*, pages 473–483. Vanderbilt University Press, Nashville, TN, 2002.
- [29] Simon Willerton. Heuristic and computer calculations for the magnitude of metric spaces, 2009.
- [30] Simon Willerton. On the magnitude of spheres, surfaces and other homogeneous spaces. *Geometriae Dedicata*, 168(1):291–310, February 2013.

UNIVERSITY OF CALIFORNIA, IRVINE, DEPARTMENT OF MATHEMATICS, 340 ROWLAND HALL, IRVINE, CA 92697-3875,
USA

Email address: gpatrick@math.uci.edu